


Cloud interference analysis in the classification of MODIS-NDVI temporal series in the Amazon region, municipality of Capixaba, Acre - Brazil

*Cristiane Batista Salgado*¹ 

*Osmar Abílio de Carvalho Júnior*² 

*Roberto Arnaldo Trancoso Gomes*³ 

*Renato Fontes Guimarães*⁴ 

Abstract

This research aimed to analyze MODIS-NDVI time series classifications, with three different algorithms, seeking to identify the ideal amount of images for studies in environments with high cloudiness rates. The spatial cut used for the study was the municipality of Capixaba, located in the state of Acre in the Amazon region. For each NDVI image, a cloud mask was constructed. This mask allowed to organize the temporal cube by cloud coverage quantity. Thus, the impact of eliminating high cloud images for the series classification was tested. At each cut, the temporal cube was redone, evaluating results for a new set of bands. For the accuracy analysis, the Kappa coefficient was adopted. A total of 84 classifications were made. Three classification algorithms (Minimum Distance, Spectral Angle Mapper and Spectral Correlation Mapper) and 4 different interactions between classes and samples were tested. Over the period analyzed, approximately 80% of images showed cloud cover above 90%. The tests showed that the removal of the images with cloud increased the quality of the classification, and the best results were found in small cubes (10 to 35 images) and with low cloud cover (0 to ~ 6%). The Minimum Distance algorithm presented the lowest coefficient of variation, showing a lower sensitivity to the presence of clouds.

Keywords: Cloud cover. Time series. Amazon

¹Instituto Federal de Brasília (Federal Institute of Brasilia), Brasilia, Distrito Federal, Brazil. cristiane.salgado@ifb.edu.br

²University Brasilia, Brasilia, Distrito Federal, Brazil. osmarjr@unb.br

³University Brasilia, Brasilia, Distrito Federal, Brazil. robertogomes@unb.br

⁴University Brasilia, Brasilia, Distrito Federal, Brazil. renatofg@unb.br

Article received on: Feb 08, 2019. Accepted for publication: Aug 12, 2019.

Introduction

Spatial analysis of geographical data can be used to measure properties, dynamics and relations, considering the spatial location of phenomena (CÂMARA et al., 2002). Geotechnologies, applied to spatial analyses, brought the possibility of representation and monitoring of the diverse dynamics of the Earth's surface, accelerating the availability of data in time (FITZ, 2008). Through these technologies, researchers can observe transformations in land use and occupation, hydrographic dynamics, urban growth, the monitoring of agricultural crops, burnings, and deforestation, in addition to generating, for example, vegetation indices (HUETE et al., 2002).

The availability of time series that are completely free of noise depends on the climatic conditions of the regions, which limits the information available for some areas of the globe (BRASWELL et al., 2003). Monitoring temporal curves of the various land surface targets allow them to be differentiated in the mappings, in addition to enabling the management of environmental resources and agricultural production (MASSEY et al., 2017).

In the Amazon, these analyses are hindered by frequent cloud cover, which directly affects the images from optical sensors (ASNER, 2001). Although remote sensing by satellites provides a viable means of observing the Amazon in a spatially wide and temporally frequent manner, the optical evaluation of tropical areas is compromised by the high concentration of aerosols (biomass burning) and clouds (ALI; DE BIE; SKIDMORE, 2013; ARTAXO et al., 2013; ASNER, 2001; CHEN et al., 2004; HILKER et al., 2015; MARTINS et al., 2018).

High temporal resolution sensors increase the probability of acquiring noise-free images throughout the year for studies that entail the detection of changes. The moderate resolution imaging spectroradiometer (MODIS) sensor provides images every one or two days at a spatial resolution of 250 m (LATORRE et al., 2003; SHELDON; XIAO; BIRADAR, 2012). Its high

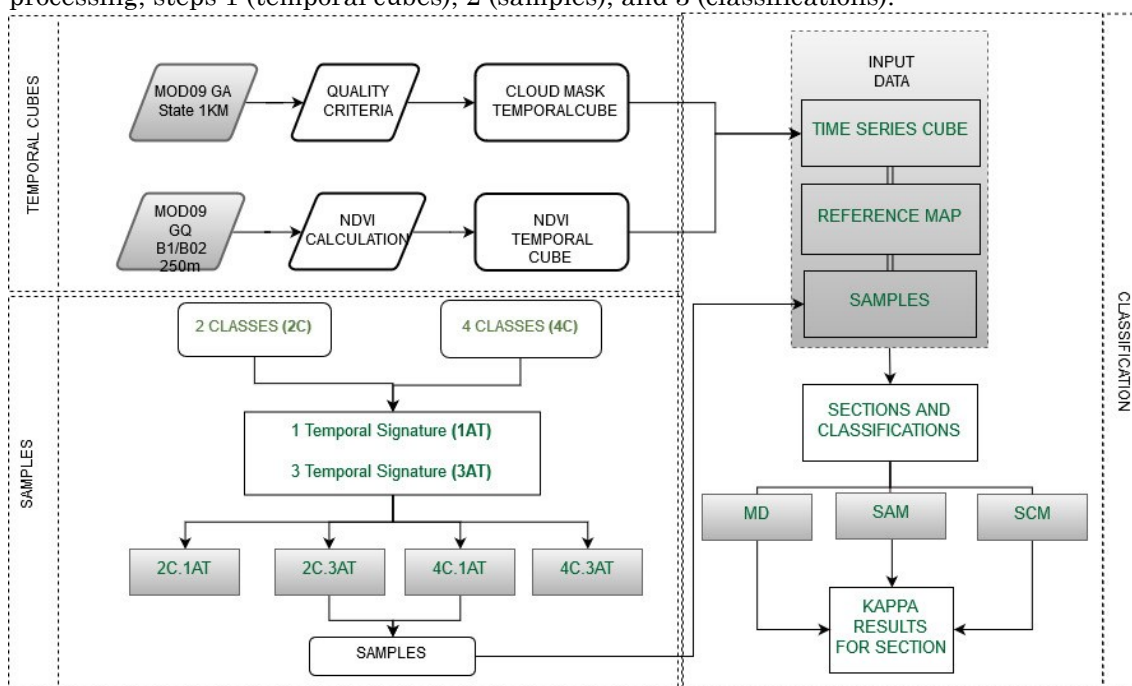
temporal resolution may fill gaps in other sensors (caused by cloud cover), such as the thematic mapper (TM) sensor, providing more information for various studies (LI et al., 2018).

Most of the cloud-free images available for the Amazon are in the dry period, particularly from July to September. In the rainy season, there is an increase in cloud coverage (MARTINS et al., 2018), directly impacting the time series analysis. The present study aimed to evaluate land use and occupation classifications in MODIS data using the ideal number of images to be used in a time series to ensure the best results.

Materials and methods

The methodological steps of the study can be organized into three processes (Figure 1). The first step is the construction of the NDVI (normalized difference vegetation index) and cloud mask temporal cubes. The second step is the choice of samples and work classes. The third step refers to the classification tests performed in the Abilius® software. These steps will be described below.

Figure 1 - Flowchart of the methodological stages of the study with respect to data processing; steps 1 (temporal cubes), 2 (samples), and 3 (classifications).



Source: authors, 2018.

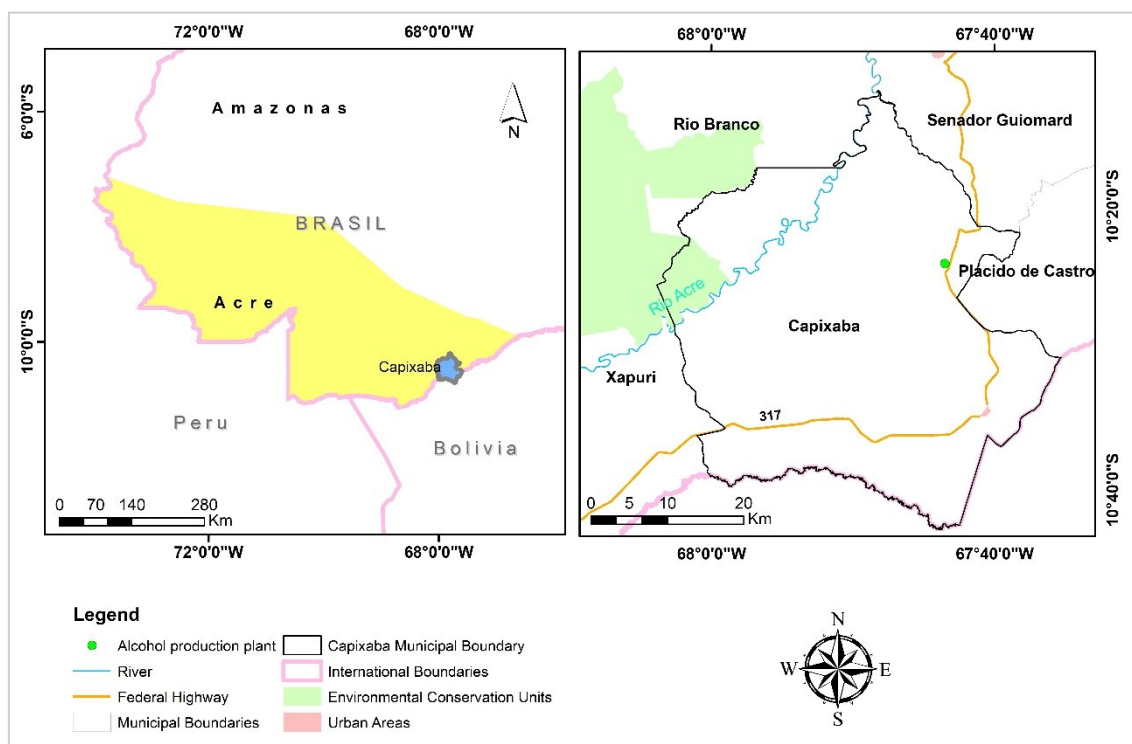
Study area

The study area is a section that involves the municipality of Capixaba and portions of the municipalities of Plácido de Castro, Senador Guiomar, Xapuri and Rio Branco, in the State of Acre, Brazil (Figure 2). The municipalities of Capixaba, Senador Guiomard and Plácido de Castro exhibit concentrations of sugarcane plantations along highway BR-317, areas near the Usina Álcool Verde. The contour is chosen to consider these dynamics in the classification tests.

The municipality of Capixaba has 47.83% of its forest cover preserved, Senador Guiomar has 28.01% and Plácido de Castro has 25.98% (INPE, 2017). Agricultural activity is a significant part of the municipalities' gross domestic product (GDP), with 45.02% in Capixaba, 31.07% in Senador Guiomar and 28.75% in Plácido de Castro, in the year 2015 (IBGE, 2016). Cattle in the municipality of Capixaba number 155,881 heads, and the main crops in 2015 were sugarcane (174,180 tons in 2,903 ha), maize (5,396 tons in

1978 ha) and cassava (31,207 tons in 1,172 ha) (IBGE, 2016). In 2015, the neighbouring municipalities Senador Guiomar and Plácido de Castro contributed to the production of sugarcane because of their proximity to the ethanol plant, contributing 4,785 and 525 tons, respectively. (IBGE, 2016).

Figure 2 - Map of the study area location.



Source: Digital data from the Economic Ecological Zoning of the State of Acre.

Org: authors, 2018.

MODIS sensor data

The MODIS sensor has been in operation since 2000 aboard the Terra platform and since 2002 on the Aqua platform, providing global images twice a day. Its spatial resolution ranges from 250 m to 1 km, with 36 spectral bands. In addition, the data can be accessed free of charge through the website Earth Data/NASA (National Aeronautics and Space Administration).

Two MODIS products are used: (a) the MOD09GQ product with daily data for the area of interest, containing bands 1 and 2 (red and infrared) at a resolution of 250 m to generate the NDVI; and (b) the MOD09GA product containing daily images with a resolution of 1 km over the quality of the images, enabling the creation of the cloud mask (VERMOTE, 2011; DAAC; FALLS, 2014)

The NDVI is sensitive to chlorophyll, to interferences related to variations of the angle of the sun, and to atmospheric effects (SANTANA et al., 2010). The calculation of this index is as follows:

$$NDVI = \frac{\rho \text{ IVP} - \rho \text{ V}}{\rho \text{ IVP} + \rho \text{ V}}$$

where $\rho \text{ IVP}$ is the reflectance in the near-infrared (800 - 1100 nm) and $\rho \text{ V}$ is the reflectance in the red range (600 - 700 nm).

To describe the cloud masks, the following criteria were chosen: the cloud state (clear), the aerosol quantity (climatology and low) and the cirrus detection (none and small). The mask was resampled at 250 meters so that the NDVI images were compatible. Both products were obtained from August 2014 to July 2015.

It is common to filter the time series of the MODIS sensor, e.g., with a median filter, to eliminate noise (DE CARVALHO JUNIOR et al., 2008; DE CARVALHO JÚNIOR et al., 2012). In the present study, it was decided not to filter the data to maintain the exact relation between the mask pixel and the NDVI image pixel; filtering could change those values.

Temporal classification

In the present study, the temporal classification tests considered two classes (forest and non-forest) and four classes (forest, pasture, sugarcane, and water) of land use and cover. In addition, the temporal signatures used in the training were obtained through two procedures: (a) the conversion of the classes of the reference map in regions of interest in the NDVI cube, extracting the mean temporal signature of each class; and (b) the same regions of interest were processed by the module "N-Dimensional Visualiser" of the Envi 5.0 software for the selection of three temporal signatures that

represented the main variations of the sample (ABADE et al., 2015). Four combinations were thus performed for the classification tests: (a) four classes with three temporal signatures (4C3AT); (b) four classes with one temporal signature (4C1AT); (c) two classes with three temporal signatures (2C3AT); and (d) two classes with one temporal signature (2C1AT) (Figure 1).

We developed a specific module of the Abilius® software that works concurrently with the cloud mask, the NDVI cube, the temporal signatures, the data classification and the accuracy (Figure 1). First, the algorithm calculates the percentage of clouds in each NDVI scene according to the cloud mask data. Then, the NDVI cube is automatically sorted from highest to lowest percentage of cloud coverage. The method performs a series of classifications, where the first classification (point 0) considers the entire time series, while the others perform subsequent sections of the images with greater cloud interference in a linear sequence, considering a range of images determined by the user. The software allows the selection of three classifiers: the minimum distance (MD), the spectral angle mapper (SAM) and the spectral correlation mapper (SCM), which were evaluated in this study. The different sequences of temporal classifications were compared with the reference map using the kappa coefficient, which is widely used in the accuracy analysis of remote sensing image classifications (MELLO et al., 2011; CHEN et al., 2015). The kappa coefficient uses a discrete multivariate technique that considers all the elements of the confusion matrix (CONGALTONS, 1991; FONSECA, 2000). Regarding the minimum acceptable levels of this coefficient, they can vary from very poor to excellent (LANDIS; KOCH, 1977), with values between 0 and 1 (Table 1).

The reference map was an update of the land use and land cover map of 2011 (developed by the Acre Institute of the Environment using Rapdeye images) from the visual interpretation using Landsat 8 images (scene 002/67, August 2015). The sugarcane areas were surveyed in a field study conducted during October 2015 (Figure 3). A total of 84 classifications were performed

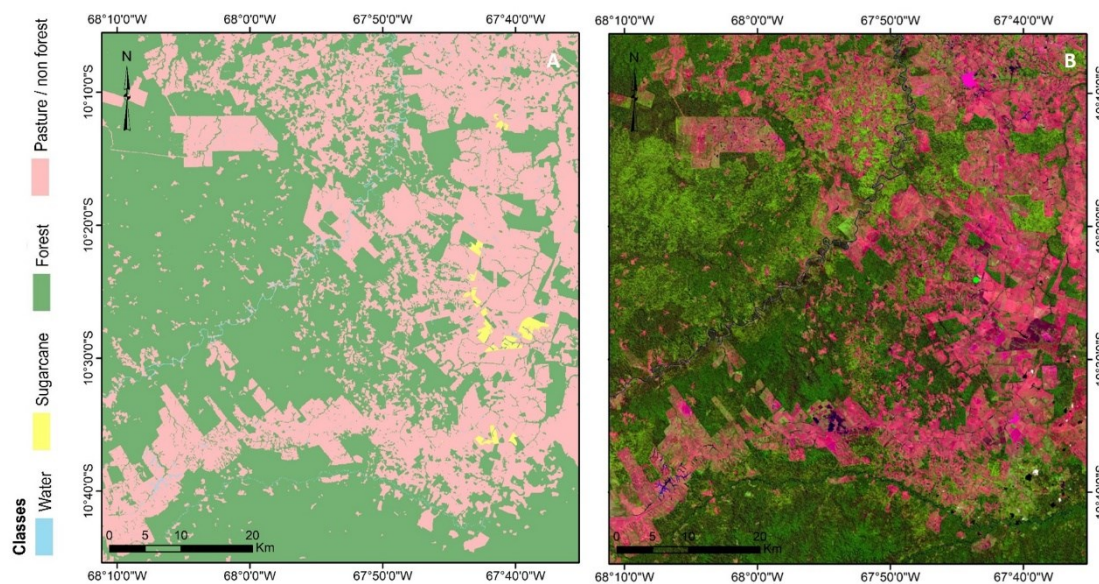
for each algorithm (MD, SAM, and SCM) and for each established combination (4C3AT / 4C1AT / 2C3AT / 2C1AT).

Table 1 - Performance levels of the kappa index.

Kappa index (k)	Performance classes
$k < 0$	Very bad
$0 < k \leq 0.2$	Bad
$0.2 < k \leq 0.4$	Reasonable
$0.4 < k \leq 0.6$	Good
$0.6 < k \leq 0.8$	Very good
$0.8 < k \leq 1.0$	Excellent

Source: Landis, Koch, 1997. Adapted by the authors, 2018.

Figure 3 - (A) Reference map used for rating validation and (B) Landsat image used in map update - composition 654, August 6, 2015.



Source: Environment Institute of Acre (Instituto de Meio Ambiente do Acre- IMAC). United States Geological Survey - USGS.
Org: authors, 2018.

Results

As expected, the time sequences of the kappa coefficient showed a significant initial climb, disregarding images with higher cloud cover until reaching stable levels, with, finally, a gradual decrease with the decrease of

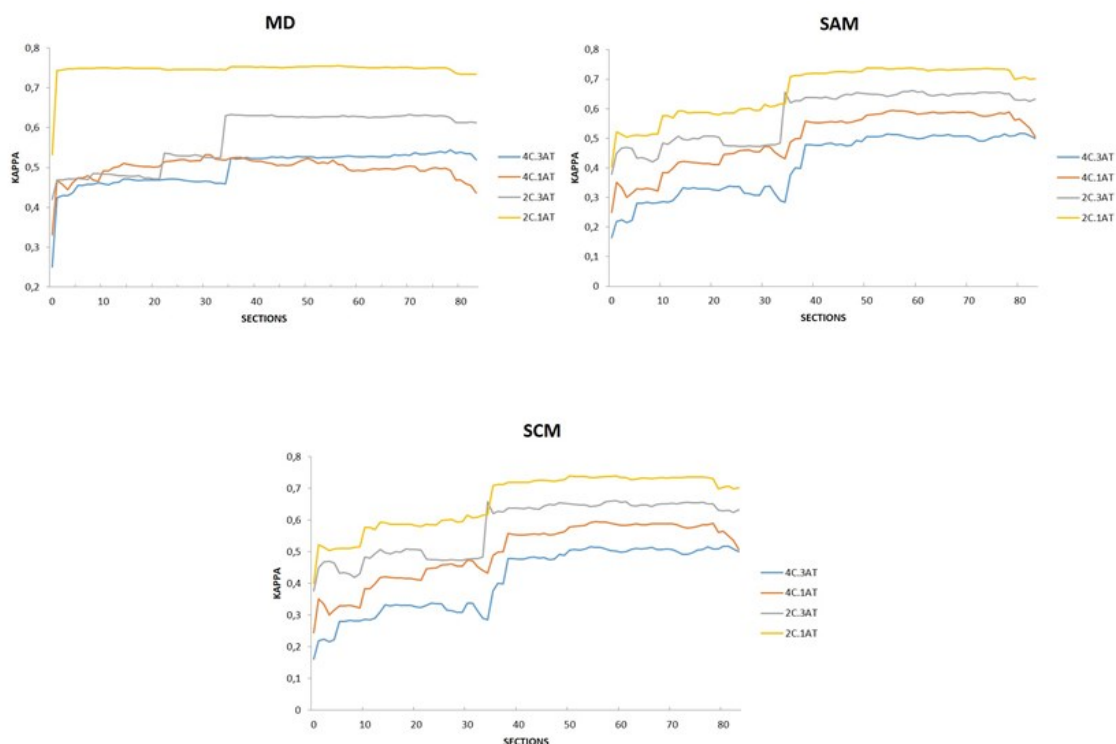
temporal information (Figure 4). Classifications with two classes (forest and non-forest) yielded better results than classifications with four classes, demonstrating the difficulty of separating the classes contained in the non-forest class. Moreover, in the majority of the tests, the models with only one mean temporal signature had better results than three models with variations from the same sample.

Among the classifications, the 2C1AT model using the MD algorithm obtained the highest kappa coefficient at 0.755 (very good performance level), selecting 34 images of the temporal cube (section 56) with cloud cover ranging between 0 and 5.62%. In this combination, a different behavior of the other models was evident. That is, from section 1, when the images with 90% or more of clouds were eliminated, the kappa coefficient was greater than 0.7, showing the efficiency of the classifier under different conditions (Figure 4). The 2C3AT model with the MD algorithm achieved a kappa coefficient of 0.632, with the selection of 20 images in the temporal cube (section 70). However, the best kappa coefficient in combinations with four classes was obtained when three temporal signatures (0.544) were used rather than one signature (0.532), selecting section 78 with only 12 images in the cube (Table 2). This was the only model where the use of three temporal signatures surpassed that of one signature, with the other variables in the same combinations.

The SAM and SCM algorithms showed similar behavior with respect to the sections and the combinations (Figure 4). There was an increase in the kappa coefficient for each section, with small variations (0.01 to 0.02). From section 35, the kappa coefficient was relatively stable for combinations with two classes and, from section 38, for combinations with four classes. Composition 2C1AT had the best kappa coefficient of 0.738, found in section 59 with a time series of 31 images with cloud coverage ranging from 0 to 3.45% (Table 2). The SAM and SCM classifiers were better than the MD classifier in the 2C3AT and 4C1AT models (Figure 5). In the 4C1AT model, the SAM

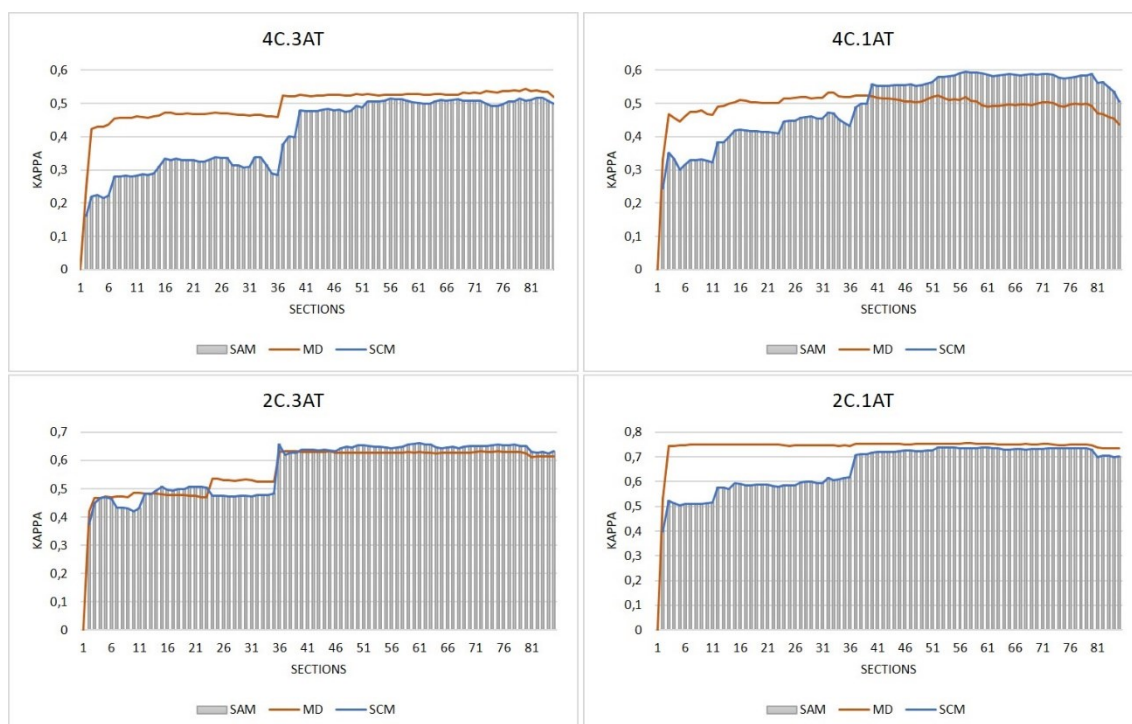
and SCM classifiers increased with each section, surpassing the MD classifier, which remained practically stable throughout the sections (coefficient of variation of 5.46).

Figure 4 – The kappa coefficients resulting from classification with the MD, SAM and SCM algorithms, by section and by combination: 4C3AT; 4C1AT; 2C3AT; 2C1AT.



Source: authors, 2018.

Figure 5 - Comparison of SAM, SCM and MD classifiers with combinations of four and two classes



Source: authors, 2018.

Table 2 - Best kappa coefficient per algorithm (MD, SAM, and SCM) and combination.

Analysis (a)	MD			
	4C3AT	4C1AT	2C3AT	2C1AT
Larger kappa	0.544	0.532	0.632	0.755
Section number	78	31	70	56
Number of images in the cube*	12	59	20	34
% cloud coverage**	0	54.13	0.07	5.62
Kappa in section 0	0.24	0.33	0.41	0.53
Analysis (b)	SAM/SCM			
	4C3AT	4C1AT	2C3AT	2C1AT
Larger SAM kappa	0.516971	0.594528	0.661072	0.738362
Larger SCM kappa	0.516997	0.594627	0.661100	0.738364
Section number	80	55	59	59
Number of images in the cube*	10	35	31	31
% cloud coverage**	0	5.91	3.45	3.45
Kappa in section 0 - SAM	0.164525	0.249362	0.377521	0.404186
Kappa in section 0 - SCM	0.161943	0.243831	0.376299	0.399313

* Number of images remaining in the cube after section. ** Maximum percentage of cloud coverage in the resulting cube images.

Source: authors, 2018.

Of the three algorithms, the lowest mean kappa coefficient was obtained with the SCM (0.411) in the 4C3AT combination (Table 3). The highest standard deviation was observed in the same combination for the SCM and SAM algorithms (0.103). The largest coefficients of variation were observed for the SCM and SAM algorithms, all of which are greater than 12%. The lowest coefficient of variation was observed for the MD algorithm in the 2C1AT combination.

Table 3 - Analysis of means, standard deviation and coefficient of variation of the data.

Algorithm	Measures	4C3AT	4C1AT	2C3AT	2C1AT
MD	Mean	0.498	0.498	0.573	0.747
	Standard deviation	0.044	0.027	0.069	0.024
	CV %	8.885	5.467	12.025	3.234
SAM	Mean	0.412	0.498	0.575	0.66
	Standard deviation	0.103	0.093	0.088	0.085
	CV%	25.09	18.77	15.24	12.94
SCM	Mean	0.411	0.498	0.575	0.66
	Standard deviation	0.103	0.094	0.088	0.086
	CV%	25.11	18.81	15.24	12.97

Source: authors, 2018.

In the confusion matrix for section 80, using the MD algorithm and two classes (Table 4), the results showed that in the combinations that used three temporal signatures, there was more confusion between the pixels of the non-forest class. In the combinations with four classes (Table 5), there was less confusion for the water, sugarcane and forest classes when there was an increase in the number of samples. The results of the classifications show that in section 35, there was great confusion between the pasture classes (Figure 6).

Table 4. Matrix of confusion for the combinations with two classes, section 80.

Section 80		2C3AT		2C1AT		
MD	No-forest	Forest	Kappa	No-forest	Forest	Kappa
No-forest	20,692	1475	0.61	26,966	3622	0.73
Forest	12,715	43,518		6441	41,371	
SAM	No-forest	Forest	Kappa	No-forest	Forest	Kappa
No-forest	21,575	1859	0.62	25,332	3053	0.70
Forest	11,832	43,134		8075	41,940	
SCM	No-forest	Forest	Kappa	No-forest	Forest	Kappa
No-forest	21,575	1859	0.62	25,332	3054	0.70
Forest	11,832	43,134		8075	41,939	

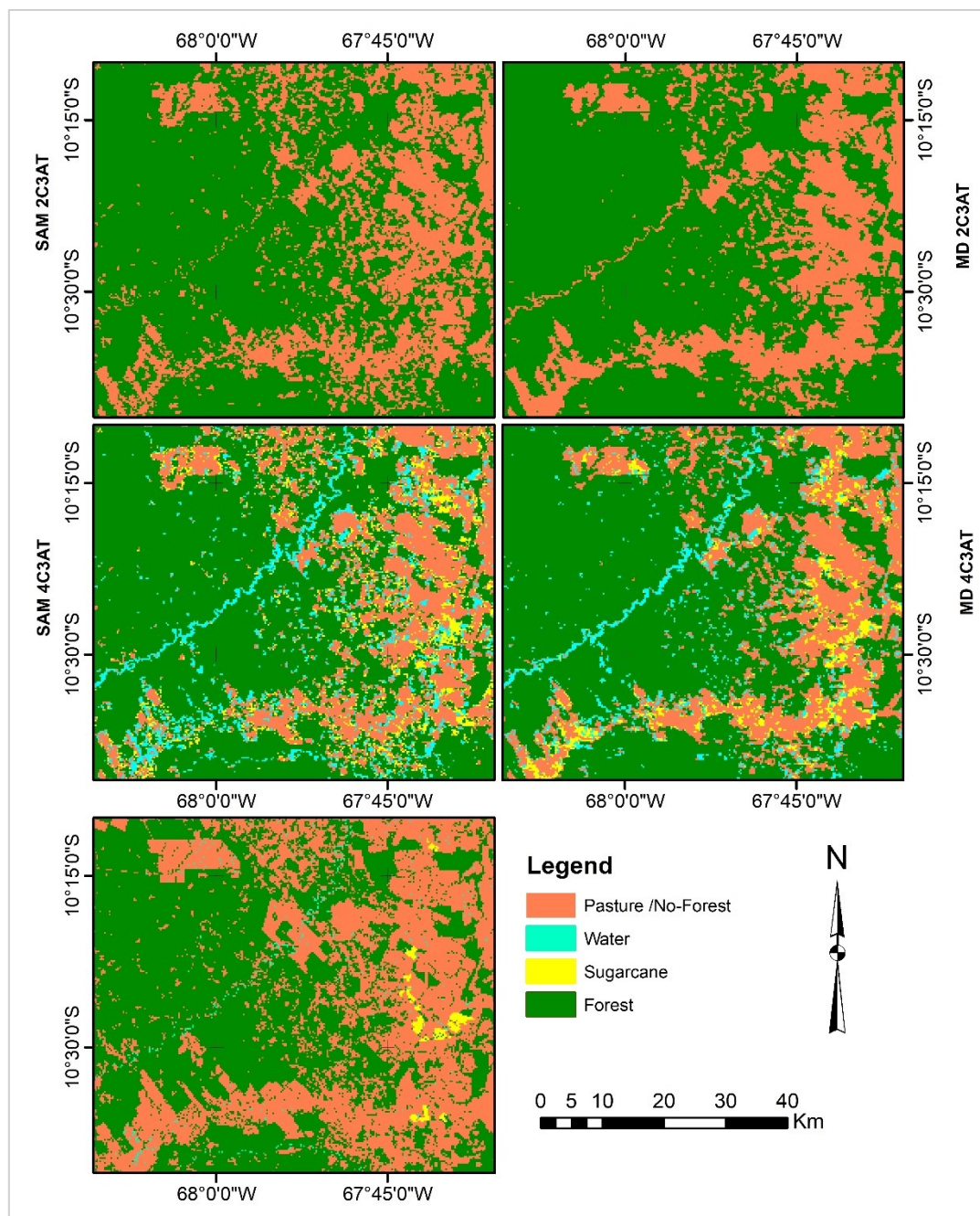
Source: authors, 2018.

Table 5 - Matrix of confusion for the combinations of four classes, section 80

Section 80		4C3AT				4C1AT				
MD	Pasture	Water	Cane	Forest	Kappa	Pasture	Water	Cane	Forest	Kappa
Pasture	16,801	202	160	1038	0.53	13,075	106	126	2738	0.47
Water	2814	181	34	963		1714	177	51	431	
Cane	2383	34	212	384		11,253	151	249	424	
Forest	10,452	107	26	42,609		6408	90	6	41,401	
SAM	Pasture	Water	Cane	Forest	Kappa	Pasture	Water	Cane	Forest	Kappa
Pasture	16,046	140	98	1155	0.51	18,297	152	116	1809	0.56
Water	3976	263	89	1178		3783	240	75	866	
Cane	3469	36	145	978		3937	35	171	1132	
Forest	8959	85	100	41,683		6433	97	70	41,187	
SCM	Pasture	Water	Cane	Forest	Kappa	Pasture	Water	Cane	Forest	Kappa
Pasture	16,047	140	98	1155	0.51	18,299	152	116	1809	0.56
Water	3976	263	89	1178		3782	240	75	866	
Cane	3469	36	145	978		3936	35	171	1132	
Forest	8958	85	100	41,683		6433	97	70	41,187	

Source: authors, 2018.

Figure 6 - Results of the 2C3AT and 4C3AT classifications (SAM and MD) in section 80.



Source: authors, 2018.

Discussion

The test results showed that the maintenance of images with clouds influenced the result of the classifications. As the cloudy images are removed,

there is an improvement in the classification results. In section 0, *i.e.* in the classification of the cube with all the images, the lowest kappa coefficients were found for all combinations, validating the strong influence of the cloud presence in the results.

The best classification results were obtained when the cubes contained 10 to 35 images over the entire period and the cloud cover was minimal, ranging from 0 to 5.91%. Among the results, the combination 4C1E using the MD algorithm was an exception, and the cube with the best kappa coefficient reached 59 images, with cloud cover ranging from 0 to 53%. Even without the best kappa coefficient (0.53), the results show that the MD algorithm is less sensitive to the presence of clouds in the time series. The low coefficient of variation in all the combinations, compared to the other algorithms, reinforced this finding.

The kappa coefficients for the algorithms tested varied with the number of land uses and land cover classes. When the number of classes increased, the kappa coefficient decreased, corroborating the results found in other studies (ABADE et al., 2015). In the tests with only two classes (forest and non-forest), the targets had very different temporal behaviors, increasing the efficiency of the algorithms (SANTANA et al., 2010). In the results for four classes, there was a greater confusion of the targets and a reduction of the kappa index. The primary confusions occurred between the sugarcane class and pasture, a fact observed in other studies with a time series classification involving sugarcane cultivation (VICENTE et al., 2012; XAVIER et al., 2006). In the case of the municipality of Capixaba, where there are large areas of pasture in contrast to sugarcane cultivation, confusion between the targets is common (XAVIER et al., 2006).

In addition, the image-section process primarily eliminates images from the rainy season because of the increased cloud cover, preferentially agglutinating the images available in the dry season series (June to August). Therefore, the seasonal representation of plant phenology may be impaired,

with little representation of the rainy season. In addition, sugarcane harvest occurs in June and July for the species cultivated in the State of Acre (AMARAL et al., 2001; BARDALES et al., 2011). Therefore, the temporal profiles of sugarcane can be confused with pasture or secondary forest (previously deforested areas at the regeneration stage). Some sugarcane areas have their harvest period extended to the months after June and July, maintaining the vegetation coverage during the period of greater availability of images and tending to have a temporal signature similar to the secondary forest areas.

The identification of water, despite being a clearly distinct target from the others, was influenced by the special resolution of the sensor. Rivers in the study area have a narrow lateral extension, which affects the detection of bodies in this class (ABADE et al., 2015).

In the SAM and SCM algorithms, the best kappa coefficient for the classifications using four targets was 0.59, showing the ability of these algorithms to separate targets, even with a high presence of noise. Although this kappa coefficient is considered a “good” result, it may not meet the needs of studies that require better accuracy.

Therefore, the study of the time series in the Amazon is limited by the presence of clouds; however, it is possible to obtain good classifications, requiring the removal of most of the time-series images. The results were hampered by the lack of monitoring of plant cover phenology throughout the year, hindering this type of classification. The alternative for this would be the use of sensors that suffer less influence from atmospheric issues, such as radar images.

Final Considerations

The presence of clouds in the Amazon time series influenced the quality of the classifications. The number of samples used, the number of

classes and the classification algorithms influence the maximum number of images used to ensure the best results. The MD algorithm stood out among the two-class tests, achieving a kappa coefficient considered to be "very good". For the tests with four classes, the SAM and SCM algorithms had better performance. The best kappa coefficients were found in temporal cubes whose images had up to 5% cloud coverage, being the determinant for the choice of clear, cloud-free images for the time-series studies.

Acknowledgments

The authors thank the Graduate Program in Geography of the University of Brasilia and the Federal Institute of Education, Science and Technology of Brasilia.

References

- ABADE, N. A. et al. Comparative analysis of MODIS time-series classification using support vector machines and methods based upon distance and similarity measures in the Brazilian cerrado-caatinga boundary. **Remote Sensing**, v. 7, n. 9, p. 12160–12191, 2015. <https://doi.org/10.3390/rs70912160>
- ALI, A.; DE BIE, C. A. J. M.; SKIDMORE, A. K. Detecting long-duration cloud contamination in hyper-temporal NDVI imagery. **International Journal of Applied Earth Observation and Geoinformation**, v. 24, n. 1, p. 22–31, 2013. <https://doi.org/10.1016/j.jag.2013.02.001>
- AMARAL, E. F. et al. Aptidão do solos do Acre para o cultivo da cana-de-açúcar. **Comunicado Técnica Embrapa**, v. 143, p. 1–6, 2001.
- ARTAXO, P. et al. Atmospheric aerosols in Amazonia and land use change: from natural biogenic to biomass burning conditions. **Faraday Discussions**, v. 165, n. 0, p. 203–235, 2013. <https://doi.org/10.1039/c3fd00052d>
- ASNER, G. P. Cloud cover in Landsat observations of the Brazilian Amazon. **International Journal of Remote Sensing**, v. 22, n. 18, p. 3855–3862, 2001. <https://doi.org/10.1080/01431160010006926>
- BARDALES, N. G. et al. **Zoneamento Agroclimático para Cultivo da Cana-de-açúcar em Três Municípios da Regional do Baixo Acre, Estado do Acre, Brasil**. Rio Branco: [s.n.].
- BRASWELL, B. H. et al. A multivariable approach for mapping sub-pixel land cover distributions using MISR and MODIS: Application in the Brazilian Amazon region. **Remote Sensing of Environment**, v. 87, n. 2–3, p. 243–256, 2003. <https://doi.org/10.1016/j.rse.2003.06.002>
- CÂMARA, G. et al. Análise espacial e geoprocessamento. In: **Gilberto Câmara; Clodoveu Davis; Antônio Miguel Vieira Monteiro (Org.). Introdução à ciência da geoinformação**. São José dos Campos: INPE/DPI, 2002.

- CHEN, G. et al. Spatiotemporal patterns of tropical deforestation and forest degradation in response to the operation of the Tucuruí hydroelectric dam in the Amazon basin. **Applied Geography**, v. 63, p. 1–8, 2015. <https://doi.org/10.1016/j.apgeog.2015.06.001>
- CHEN, J. et al. A simple method for reconstructing a high-quality NDVI time-series data set based on the Savitzky-Golay filter. **Remote Sensing of Environment**, v. 91, n. 3–4, p. 332–344, 2004. <https://doi.org/10.1016/j.rse.2004.03.014>
- CONGALTONS, R. G. A Review of Assessing the Accuracy of Classifications of Remotely Sensed Data. **Remote Sensing of Environment**, p. 35–46, 1991. [https://doi.org/10.1016/0034-4257\(91\)90048-B](https://doi.org/10.1016/0034-4257(91)90048-B)
- DAAC, N. L. P.; FALLS, S. MODIS Land Products Quality Assurance Tutorial : Part-1 How to find , understand , and use the quality assurance information for MODIS land products. p. 1–17, 2014.
- DE CARVALHO JUNIOR, O. A. et al. Classificação de padrões de savana usando assinaturas temporais ndvi do sensor modis no parque nacional chapada dos veadeiros. **Revista Brasileira de Geofísica**, v. 26, n. 4, p. 505–517, 2008. <https://doi.org/10.1590/S0102-261X2008000400010>
- DE CARVALHO JÚNIOR, O. A. et al. Combining Noise-Adjusted Principal Components transform and median filter techniques for denoising MODIS temporal signatures. **Revista Brasileira de Geofísica**, v. 30, n. 2, p. 147–157, 2012. <https://doi.org/10.22564/rbgf.v30i2.88>
- FITZ, P. R. **Geoprocessamento sem complicação**. São Paulo: Oficina de Textos, 2008.
- FONSECA, L. M. G. **Processamento digital de imagens**. [s.l.] Instituto Nacional de Pesquisas Espaciais (INPE), 2000.
- HILKER, T. et al. On the measurability of change in Amazon vegetation from MODIS. **Remote Sensing of Environment**, v. 166, p. 233–242, 2015. <https://doi.org/10.1016/j.rse.2015.05.020>
- HUETE, A. et al. Overview of the radiometric and biophysical performance of the MODIS vegetation indices. **Remote Sensing of Environment**, v. 83, n. 1–2, p. 195–213, 2002. [https://doi.org/10.1016/S0034-4257\(02\)00096-2](https://doi.org/10.1016/S0034-4257(02)00096-2)
- IBGE, I. B. DE G. E E. **Produção Agrícola Municipal 2015**Rio de JaneiroIBGE, 2016. Available in: <<http://www.ibge.gov.br/estadosat/perfil.php?sigla=ac>>
- INPE. **PRODES: Desflorestamento nos Municípios da Amazônia Legal para o ano de 2017**Instituto Nacional de Pesquisas Espaciais (INPE), , 2017. Available in: <<http://www.dpi.inpe.br/prodesdigital/prodesmunicipal.php>>
- LANDIS, J. R.; KOCH, G. G. The Measurement of Observer Agreement for Categorical Data. **Biometrics**, v. 33, n. 1, p. 159–174, 1977. <https://doi.org/10.2307/2529310>
- LATORRE, M. L. et al. Sensor Modis: Características Gerais e Aplicações. **Espaço & Geografia**, v. 6, p. 91–121, 2003.
- LI, L. et al. Monitoring the dynamics of surface water fraction from MODIS time series in a Mediterranean environment. **International Journal of Applied Earth Observation and Geoinformation**, v. 66, n. November 2017, p. 135–145, 2018. <https://doi.org/10.1016/j.jag.2017.11.007>
- MARTINS, V. S. et al. Seasonal and interannual assessment of cloud cover and atmospheric constituents across the Amazon (2000–2015): Insights for remote sensing and climate analysis. **ISPRS Journal of Photogrammetry and Remote Sensing**, n. October 2017, p. 0–1, 2018. <https://doi.org/10.1016/j.isprsjprs.2018.05.013>
- MASSEY, R. et al. MODIS phenology-derived, multi-year distribution of conterminous U.S. crop types. **Remote Sensing of Environment**, v. 198, p. 490–503, 2017. <https://doi.org/10.1016/j.rse.2017.06.033>
- MELLO, M. P. et al. Spectral-temporal analysis by response surface applied to detect deforestation in the Brazilian Amazon. **2011 6th International Workshop on the Analysis of Multi-Temporal Remote Sensing Images, Multi-Temp 2011 - Proceedings**, n. 1, p. 89–92, 2011. <https://doi.org/10.1109/Multi-Temp.2011.6005055>

- SANTANA, O. A. et al. Modelagem de espectros temporais NDVI-MODIS, no período de 2000 a 2008, na bacia do Rio Paracatu, Brasil. **Revista Brasileira de Geofísica**, v. 28, n. 1, p. 47–60, 2010. <https://doi.org/10.1590/S0102-261X2010000100004>
- SHELDON, S.; XIAO, X.; BIRADAR, C. Mapping evergreen forests in the Brazilian Amazon using MODIS and PALSAR 500-m mosaic imagery. **ISPRS Journal of Photogrammetry and Remote Sensing**, v. 74, p. 34–40, 2012. <https://doi.org/10.1016/j.isprsjprs.2012.07.003>
- VERMOTE, E. F. MODIS Surface Reflectance User ' s Guide. **Orbit An International Journal On Orbital Disorders And Facial Reconstructive Surgery**, p. 1–40, 2011.
- VICENTE, L. E. et al. Séries temporais de NDVI do sensor SPOT Vegetation e algoritmo SAM aplicados ao mapeamento de cana-de-açúcar. **Pesquisa Agropecuária Brasileira**, v. 47, n. 9, p. 1337–1345, 2012. <https://doi.org/10.1590/S0100-204X2012000900019>
- XAVIER, A. C. et al. Multi-temporal analysis of MODIS data to classify sugarcane crop. **International Journal of Remote Sensing**, v. 27, n. 4, p. 755–768, 2006. <https://doi.org/10.1080/01431160500296735>



This is an Open Access article distributed under the terms of the Creative Commons Attribution License, which permits unrestricted use, distribution, and reproduction in any medium, provided the original work is properly cited.